Heliyon 10 (2024) e23557

Contents lists available at ScienceDirect

Heliyon

journal homepage: www.cell.com/heliyon

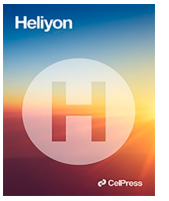

Modelling groundwater pollutant transfer mineral micropollutants in a multi-layered aquifer in Burkina Faso (West African Sahel)

Moussa Diagne Faye [a,*], Vini Yves Bernadin Loyara [b], Angelbert Chabi Biaou [a], Roland Yonaba [a], Mahamadou Koita [a], Hamma Yacouba [a]

[a] *Laboratoire Eaux, Hydro-Systèmes et Agriculture (LEHSA), Institut International d'Ingénierie de l'Eau et de l'Environnement (Institut 2iE), 1 Rue de la Science, 01 BP 594, Ouagadougou 01, Burkina Faso*

[b] *Laboratoire d'Analyse Numérique, Informatique et de Biomathématiques (LANIBIO), Université Joseph KI-ZERBO, 03 BP 7021, Ouagadougou 03, Burkina Faso*

ARTICLE INFO

Keywords:
Inferential statistics
Groundwater modelling
Micropollutants
MT3D
Multi-layered aquifer
Water quality

ABSTRACT

In Burkina Faso, human activities around water points in rural areas affect groundwater resources, which become unfit for consumption. Nearly 33.5% of boreholes are subject to point source pollution. The assessment of the evolution of such pollution should be monitored to assess groundwater quality. In addition, withdrawals for irrigation alone are estimated at 85%, i.e. 46% of the water demand, heightening the deterioration in quality while creating depression zones further leading to an increase in recharge. It is therefore critical to understand the evolution and fate of the transfer of pollutants in such environments. In this study, we aimed to model the transfer of pollutant and predict the future state of pollution using the MT3D-USGS Groundwater Solute Transport Simulator code through the Groundwater Modelling Software (GMS) over the period 2012–2062 (50 years). A mathematical model is further developed through inferential statistics and used as a surrogate model for comparison. The results showed that deterioration in water quality was more attributable to withdrawals, especially for Cyanide (Cn) and Arsenic (As). A rather slow degradation is reported for Lead (Pb), which extends over 22 km, and Fluoride (F), which extends from 4 to 10 km due to localized recharge. A faster degradation for Cn over a distance of 2–16 km and as from 3 to 11 km is also observed because of the geological setting of the subsoil. These results might assist decision-makers for the quantitative and qualitative management of groundwater resources, and the management of the basement aquifer in the area through the establishment of protection zones.

1. Introduction

Solving the problems related to improving access to water around the world is still under discussion [1]. Indeed, the spatial distribution of water resources in the world does not favour its valorisation. The recoverable part, made up of freshwater, represents 2.5% and is essentially composed of surface water and groundwater. This part of groundwater is becoming scarce in many regions of the world, particularly in sub-Saharan Africa, while the degradation of its quality is not easily perceived. Population growth, climate change and insufficient aquifer recharge make it difficult to rely groundwater as the main source of water supply in rural areas. The

* Corresponding author.
E-mail address: moussadiagnefaye@gmail.com (M.D. Faye).

https://doi.org/10.1016/j.heliyon.2023.e23557
Received 16 June 2023; Received in revised form 5 December 2023; Accepted 6 December 2023
Available online 12 December 2023

prospection for available groundwater resources in remote an rural areas still remains at the prospective stage [2,3]. Further, anthropogenic activities around some rural water points affect groundwater resource quality, which become unsuitable for consumption. It is estimated that one third of the world's population will face to water shortage issues by 2025 according to the United Nations forum in 2006 [4], which highlights the critical need for evaluation and monitoring of water resources by both public or private authorities. The focus should be on the assessment of water quality trends in the future for effective management. Nowadays, in many regions of the world, particularly in sub Saharan Africa, decreasing trends in cumulative rainfall coupled with increasing temperatures are thought to further cause a depletion of surface water planes, therefore limiting the renewal of water resources [5–11].

A number of studies have focused on finding sustainable solutions to the problem of contaminants, and also on predicting the spatial and temporal evolution of this contamination. In Botswana, [12] showed that contamination from nuclear waste would persist for more than 6000 years by modelling groundwater contamination. [13], in Turkey, worked on the design of a pollutant transport model for a multilayer aquifer and demonstrated a 20% reduction in pollution from mining waste. The work carried out by Ref. [14] in Morocco and Gandy, [15] in England, [6,16] in Burkina Faso focused on the impact of water pollution following the exploitation of mining resources. However, the main limitation is the understanding of the geometric system and the parameters that govern the flow. Added to this is the obstacle of joining the discontinuities in the preferred water movement path, in order to understand the origin and mechanisms of the different types of pollution identified.

In Burkina Faso, a landlocked country located within the Wester Sahel, the average volume of water available is 850 m^3 per year per inhabitant, slightly below the water shortage threshold of 1000 m^3/year/inhabitant [5,17–21]. Anthropogenic activities and rock formations with a high arsenic content in the basement formations are the main sources of pollution in this context [22–25]. This can further affect water quality, making hydrochemical studies in these environments difficult and more complex due to the high levels of contaminants. This is especially a cause for concern in the Sissili sub-basin, given that some water points with arsenic-rich waters (40% in 2015) are being closed or abandoned [8,16,24].

Currently, the level of understanding of groundwater quality is very limited and the water demand in aquifers is becoming increasingly intense. The Sissili catchment area, located in South-Western Burkina Faso, has been for some time been subject to a change in land use (i.e. a disturbance of 57.84% [26]) as a result to the increase in industrial mining activities and also agriculture, which uses chemical products. In addition, withdrawals for irrigation alone are estimated at 85%, i.e. 46% of the water demand. The exploitation of the water resource is carried out through boreholes that most often capture the alterites that result from chemical alteration in relation to the in situ mineralogical composition of the bedrock and various weathering processes [27]. The study conducted by Ref. [24] showed a degradation of water quality linked to anthropic activities but also to mineralization, without further providing estimates of such environmental degradation. Among the major pollutants identified are Lead (Pb), Fluoride (F), Cyanide (Cn) and Arsenic (As), which are already known to pose serious concerns for water quality and health issues in rural communities [24]. Yet, the future evolution of such type of pollution remains poorly documented and unaddressed within the body of the scientific literature. It appears imperative to strengthen the current state of knowledge on groundwater quality for a better management and use

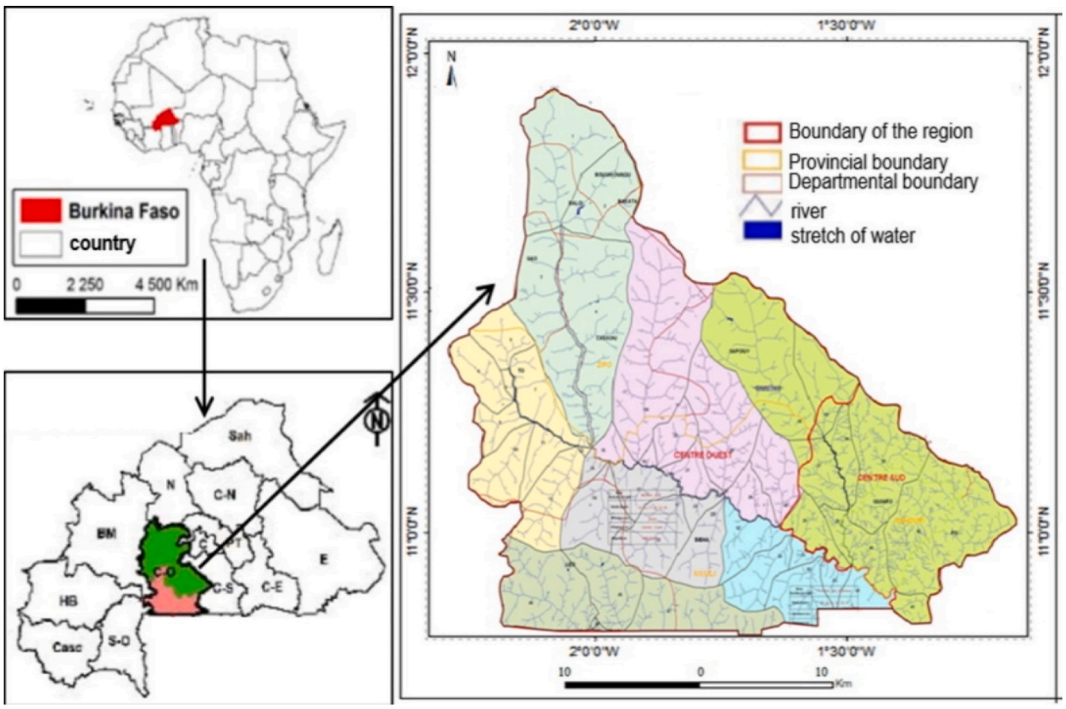

Fig. 1. Geographical location of the Sissili catchment area.

of the groundwater resource and for mitigation of health risks related to its consumption.

This study aims to assess the current state of groundwater quality as affected by micropollutants through the calibration of a groundwater simulation model code and the use of a mathematical model herein developed. The first step in this work is to develop a single-layer conceptual model in which the groundwater is connected to a river watercourse using the Groundwater Modelling Software (GMS). The model is calibrated using Dirichlet-type boundary conditions and imposed potential. A conceptualization of the transport model is further established, enabling the simulation of pollutant transport and indicating the evolution of its concentration as a function of time, i.e. diffusion and dispersion. Secondly, a mathematical model using inferential statistical evaluation techniques is used to forecast future quantities of pollutants through GMS.

2. Materials and methods

2.1. Study area

The Sissili catchment area covers an area of 7559 km^2 and is triangular in shape. It lies between longitudes 1° and 2° West and latitudes 11° and 12° North (Fig. 1) [24] and covers 12 municipalities in 3 provinces.

The relief is determined by small rocky massifs. It is a vast plain with little unevenness or dominated by plains and plateaus. It is slightly disturbed in the western part by hilly elevations varying from 249 to 425 m above the sea level and generally oriented North-South. The hydrology is strongly influenced by the altimetry.

The Sissili has three types of land use/land cover: agricultural areas, which are the most important from the point of view of spatial occupation, pastoral areas, which are vast areas of natural formations, and finally wetlands. The evolution of the land cover from 1982 to 2011 is shown in Fig. 3. It can be seen that shrub savannah is the dominant unit in 2002 and covers 40.65% of the total area. Changes in land use from 2012 to 2018 show that more than half of the total area, i.e. 57.84%, is occupied by agricultural areas [26]. There are 3 soil classes found within the catchment: poorly developed soils with hydromorphic alluvial deposits, rough mineral soils and hydromorphic soils.

The climate is characterised by an alternance of two cycles: a dry season from November to April and a rainy season from May to October. The climate is of Sudanian (South Sudanian) type, with an annual rainfall of over 900 mm. Decreasing trends in rainfall over the last two decades have been observed, with a southward migration of the 600 mm and 900 mm isohyets over the period 1931 to 2000 by approximately 100 km–150 km.

The catchment is crossed by the 322 km long Sissili river which has its source in the locality of Thyou (in the northern part of the catchment). With a slope of 1.48 m/km over the first 42 km, it flows southwards to end its course in the department of Tô in Burkina Faso before continuing towards Ghana, with a drainage density of 0.74 km^{-1} [27–30].

Regarding the geology (Fig. 4), there are two major geological units of the Proterozoic age: the plutonic unit (granite, granodiorite, micaschist) and the sedimentary volcanic unit (amphibolite, schist, rhyodacite). Rock formations with high arsenic content are also distinguished [27–30]. However, it can be distinguished into three types of geological formations that are productive in terms of water resources: migmatites, granites and basic rocks, quartz veins.

The hydrogeology (Fig. 2) is essentially covered by geological formations with low productivity. Indeed, the hydraulic productivity of the groundwater catchment structures depends on the importance of the faults which affect the bedrock and the petrographic facies.

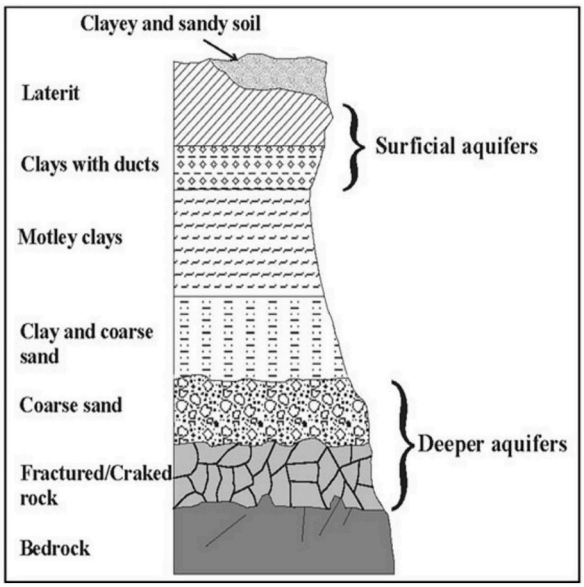

Fig. 2. Alteration profile of aquifers in the crystalline region in Burkina Faso.

In terms of hydraulic productivity, plutonic formations can provide permanent flow which exceed 20 m^3/h. Relatively, a low hydraulic productivity for volcanic sedimentary formations is observed, which allows flows of over 5 m^3/h to be obtained. Very low hydraulic productivity is observed for post-tectonic intrusive plutons, which barely deliver 5 m^3/h and lowering to 2 m^3/h when they are made of fine and homogeneous grains [24].

2.2. Sampling and analysis methods

In order to assess pollution in rural areas, a field campaign has been implemented to detect high levels of harmful chemical elements in water in various localities in Burkina Faso. The sampling methodology is based on a strategic or regional 10 km square grid covering the entire catchment according to the standard method used by geologists. Within each grid, eight (8) points are selected and evenly distributed according to geology. The number of sampling points could exceed eight depending on the land use and, more specifically, the population density per square kilometer. In this study, a number of quality parameters were analysed in order to characterise the overall water quality and to identify possible pollution. Data processing methodologies are adopted to the local conditions, although built upon existing methods [8,16,24]. The sampling was carried out in 58 boreholes equipped with human powered pumps in order to have a mesh covering all municipalities (see Fig. 4), following the recommendations of the standard methods (reference norm US EPA, 2017). To collect groundwater from a borehole drilling, it is generally advisable to carry out an intensive pumping before collecting the sample (about 20 L), or with a controlled opening sampler when sampling is carried out at the level of the wells. For each sampling point, four water samples (500 ml each) are collected in plastic bottles while five samples are collected on mining sites. For each sample, 4 parameters are measured, including Lead (F), Fluoride (F), Cyanide (Cn) and Arsenic (As). Fluoride ions (F) concentrations are obtained by the molecular absorption spectrophotometry method according to Hach 8029 (DR 3800) with a detection limit of 0.02 mg/l. Total Cyanide (Cn) is analysed by the spectrophotometric method after heat mineralization (DR 3800) with a detection limit of 0.005 mg/l. Arsenic (As) and Lead (Pb) are analysed by microwave plasma atomic emission spectrometry (in accordance with NFISO11969 and FD T90-112 norms) with detection limits of 2 µg/l and 5 µg/l respectively.

2.3. Setting up hydrodynamic and pollutant transfer models

2.3.1. Hydrogeological conceptual model

In this study, a conceptual monolayer model from the hydrogeological point of view is selected according to the availability of data. This model allows us to have an overview of the topographic surface at the edge of the aquifer. In this sense, the alterite aquifer is defined as heterogeneous, as it is a complex structure due to the presence of discontinuities [32–35]. In fact, the flow exists on the basis of the presence of fractures in these media dividing the space into a series of permeable masses, known as porous matrices [36,37]. The

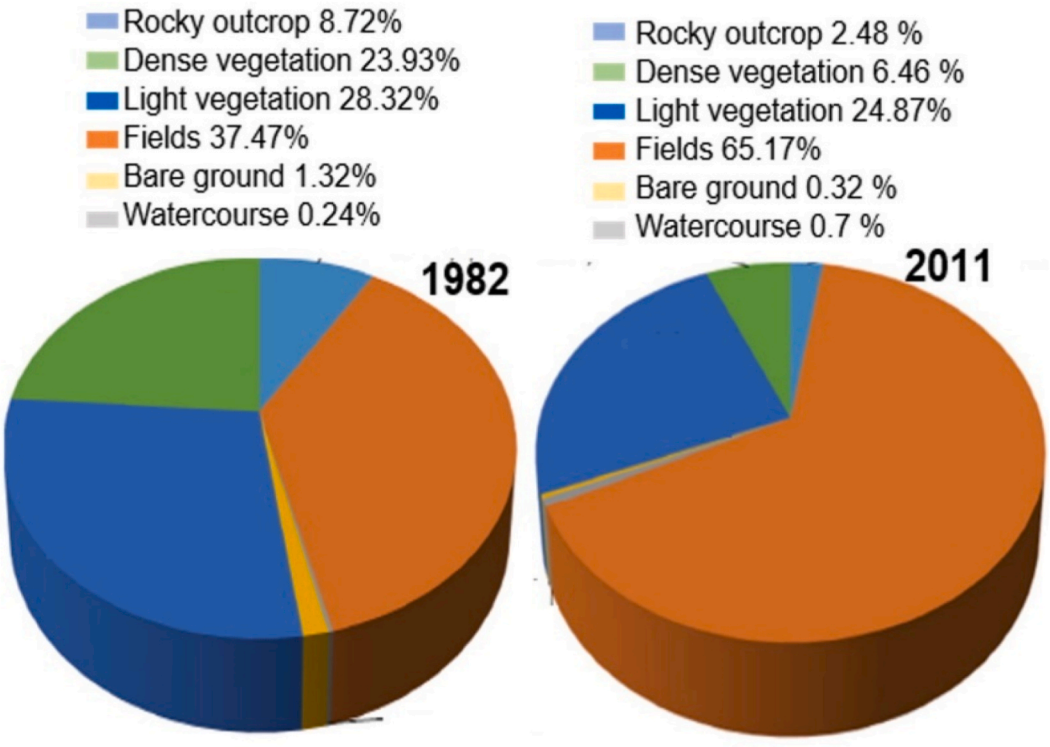

Fig. 3. Land use composition in the Sissili catchment area between 1982 and 2011.

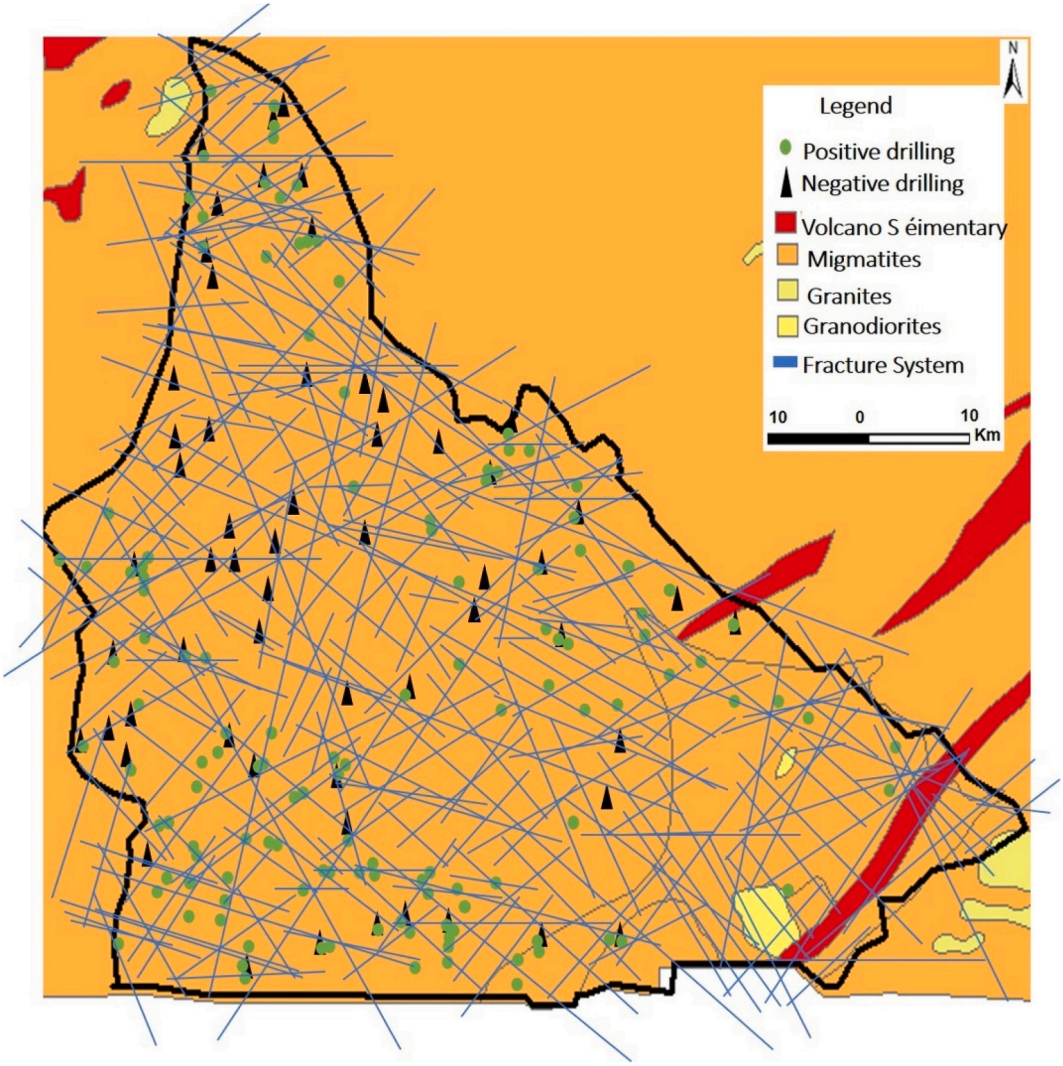

Fig. 4. Simplified geological map, distribution of fractures and water extraction points for positive boreholes [31].

existing watercourse interacts through the exchange of flows. In order to conceptualise a flow model, the geometry of the domain to be modelled is essential. The choice of the mesh is guided by the study conducted by Ref. [38]. Generally, the geological contours condition defines the generation of the mesh. In this study, the surface area to be modelled is of 7559 Km^2. Each grid covers an area of 150 m by 150 m, with a total number of 225,000 meshes of 150 m on each side. For each grid cell, the top and base altitudes of the different layers are provided for geometry criteria. Digital terrain model (DTMs), extracted from the Shuttle Radar Mission Topography (STRM), with a resolution of 30 m, have been used in this regard. The sources of groundwater recharge include precipitation, leakage from groundwater include precipitation and river input [39,40–43].

Groundwater recharge appears to be much more uniform in the southern part and from rainfall-runoff modelling studies this value is estimated at 5% of annual rainfall. The data was introduced into the model and applied to the top layer of the model. Withdrawals occurs because of human supply needs (water supply, industrial activities, crop irrigation needs and livestock watering) and are estimated at 300 m^3/day. Also, lateral groundwater flow and evapotranspiration contributes to withdrawals amounts. These uses are modelled as pumping flow. As far as the hydrodynamic parameters are concerned, and considering that the simulation is carried out under steady-state conditions, the hydraulic conductivity is the only parameter affecting the hydraulic potential field and the model flow. It is essentially determined on the basis of the geological setting and estimated from pumping tests. The hydraulic conductivity of each layer is assessed using the expression $T = K * b$ where T (in m^2/s) is the transmissivity, K (in m/s) is the hydraulic conductivity and b (in m) is the thickness of the aquifer under consideration. Given our single-layer system, equivalent values should be considered. In other words, for a given location where K values are known for each of the weathered and fissured compartments, a single value called the equivalent hydraulic conductivity is assigned to the single-layer aquifer.

2.3.2. Model boundary conditions

The boundary conditions help in defining water or solute interactions between the modelled area and neighbouring areas and also the relationship with other components of the water cycle. Usually, two types of boundary conditions for water transfer processes are used: the imposed potential or internal Dirichlet condition, which imposes that the head is equivalent on both sides of a split node in two subdomains, and the type of flux imposed, which is automatically applied to a nil (zero) value on the periphery of the model. It is however possible to impose a non-zero value where necessary.

Case in this study, the imposed potential is used and the Dirichlet conditions are solved based on the piezometry map of the sub-catchment at the boundary of the modelling area [29,30,34–38]. The crossings of the point of equal potential called isopiestic lines with the end of the area to be modelled, create nodes that are assigned the head of the corresponding isopiestic lines. The Sissili River runs through the sub-catchment and flows abundantly due to its relief and the rainfall in the area. This river is symbolised by a drain type condition which stems from the DTM (Fig. 5). The application of the MT3D code to simulate pollutant transfer leads to two different boundary conditions. The external boundary condition which considers that the recharge is set up by the Neumann-type condition. This can justify the impermeability of the bedrock in the area to be modelled, as well as the compliance with the watershed. Internal conditions are specific to pollutant transfer modelling. They also make it possible to manage exchanges between the discretized domains. The connections under horizontal domains confirm the Dirichlet conditions, which ensure that the water level is maintained at a similar level [24,44,45]. For the pollutant concentration model in our case, the conditions corresponding to constant concentrations are imposed at the level of each catchment work. This value corresponds to the concentration derived from the results of analyses carried out by Ref. [24] in accordance with the national standards. This makes it possible to reproduce real conditions, whereas for the other cells, the concentration is zero.

2.3.3. Model calibration

The calibration procedure consists in reducing the bias between the observed and simulated values through the adjustment of model parameters, here the hydraulic conductivity and groundwater recharge [36,38,46–48]. In this study, a "*trial and error*" procedure is used, in which values are manually assigned to the various parameters to achieve an optimal calibration. The error metrics used to assess the optimality of the calibrated model are the mean error (ME), the mean absolute error (MAE) and the root mean square error (RMSE), defined as in Equations (1)–(3)s.

$$\mathrm{ME} = \frac{1}{n}\sum_{i=1}^{n}(h_m - h_c)_i \tag{1}$$

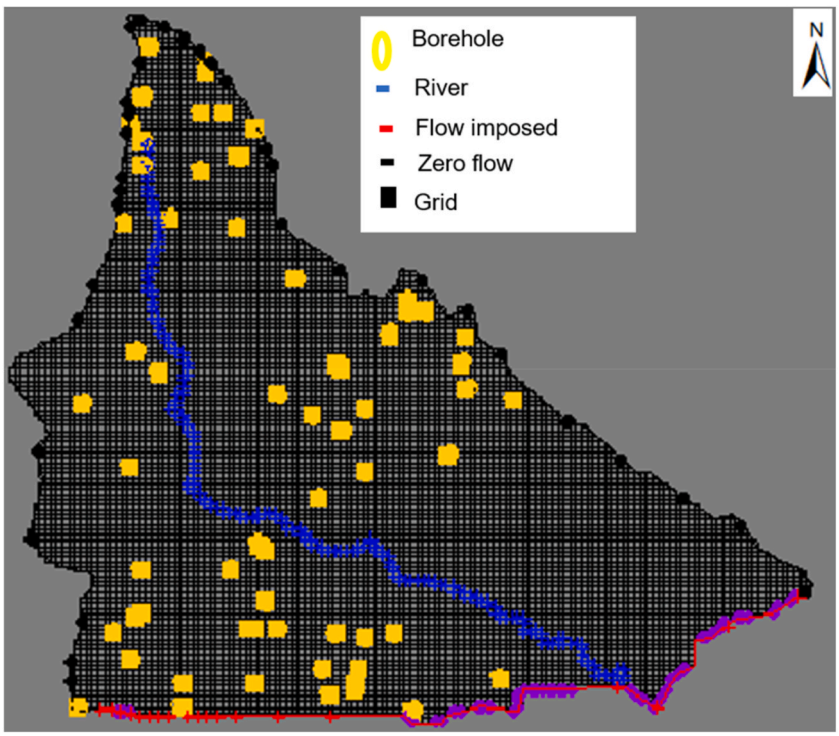

Fig. 5. Grid size and boundary conditions in the study area.

$$\mathrm{MAE} = \frac{1}{n}\sum_{i=1}^{n} |h_m - h_c|_i \tag{2}$$

$$RMSE = \sqrt{\frac{1}{n}\sum_{i=1}^{n} (h_m - h_c)_i^2} \tag{3}$$

In the case of this study, the model is deemed to be satisfactorily calibrated when an error of 2 m maximum and a confidence level of 96% are reached. The calibration was done using the data from the year 2019, since they were the most recent and complete data.

2.3.4. Sensitivity testing

The sensitivity testing was employed to identify how the model parameters control the dynamics of groundwater flow in the study area. The hydraulic conductivities are reduced by 10% and further increased by 10% of their calibrated values in this regard. This choice was made because, during calibration, the slightest change in conductivity value is likely to have an impact on piezometry, unlike groundwater recharge. The recharge was reduced by 30% and further increased by 30% of its initial value. The relative sensitivity coefficient Sr is therefore calculated to quantify the relative effect of the different model parameters.

A positive (negative) Sr indicates that the simulated variable increases (decreases) with an increase in the model parameter value. The higher the Sr (in absolute value), the more sensitive the model is to the parameter being tested. Equation (4) was used to compute the Sr coefficient:

$$S_r = \left[\frac{F' - F_{ref}}{F_{ref}}\right] \Big/ \left[\frac{X' - X_{ref}}{X_{ref}}\right] \tag{4}$$

2.4. The solute transport MT3D code

The conceptualization of the transport model refers to the quantitative reproduction of the transport system, which summarizes the collective aspects of the contaminant source and its evolution [49–51]. The objective of a pollutant transport study is to be able to take into account the temporal evolution between pollutants [38,52]. This refers first of all to the quantification of the pollutant and its progression from the surface to underground percolation. In this work the steady state hydrodynamic model is defined and coupled to the transport model [36,52].

The preservation of the resource requires a good understanding of the processes of transfer or transport of pollutants. The model simulates the transfer of pollutant for different properties given in advance and indicates the evolution of its concentration as a function of time within the aquifer [49,53,54]. The parameters used in the modelling are advection (which is associated with the permeability coefficient parameters) and porosity. During this transport, the unidirectional flow is the product of the quantity of water that circulates by the concentration of the dissolved solute [48] as described by Equation (5):

$$\frac{\partial \theta C}{\partial t} = -\nabla \mathrm{qCtotal} = -\nabla\ (\mathbf{CV}\text{-}\boldsymbol{\theta}\mathbf{D}\nabla \mathrm{C}) \tag{5}$$

where C is the concentration of the pollutant, qC total = ($C\mathbf{V}$ - $\boldsymbol{\theta}\mathbf{D} \cdot \nabla C$) is the amount of pollutant transported by advection and dispersion, D is the dispersion coefficient, -∇ qC total denotes the flux of the quantity of pollutant, $\boldsymbol{\theta}C$ the mass of pollutant per unit medium and $\partial\boldsymbol{\theta}C/\partial t$ denotes the ratio at which this quantity becomes important. Dispersal is at the source of the spread of contamination and contributes to the dilution of concentrations. It is associated with the parameters of a longitudinal dispersion coefficient D_L (whose value is 1/10th of the length of the pollutant plume or observation) and a transverse dispersion coefficient D_T (whose value is 1/100th of the length of the pollutant plume or observation) [55–57]. These values are generally proportional to the Darcy velocity, and an upward directed vertical dispersion coefficient and is very low, as shown in Equation (6).

$$D_L = \alpha_L U \text{ and } D_T = \alpha_T U \tag{6}$$

In this study, no laboratory tests have been carried out in the area. The predicted dispersion values were evaluated according to the commonly used dimensional based procedure. This procedure initially designs a longitudinal dispersion coefficient equal to 0.1 times the distance travelled by the pollutant. This is only an assessment that generally suggests a reliable starting point for modelling. Previous studies [14,37,57–59] define through experiments that the coefficients responsible for the spreading of a pollution along the flow directions are taken by considering that α_L equals to 1/10th of the length and α_T equals 1/20th of the length. In this study this value is considered to be equal to 2.

2.5. Simulation of pollutant transport

To simulate pollutant transport, we assigned concentration levels to the different pollutant determined (mg/l) in the study area and corresponding to the concentrations obtained by the 2012 campaign. The different pollutants are taken for simulation in this study. Only concentrations which exceed the authorized drinking water standards in Burkina Faso are considered as they are the sources of pollution in the environment. First, the current state of pollution is presented for Cn, Pb, F and As. Through this modelling effort, a risk-assessment prediction tool is developed for an optimal management of the water resource in the study area. The conditions

corresponding to constant concentrations are imposed at each catchment work. This allows us to reproduce the conditions in 2012 to determine the actual fate of the pollutant in 50 years.

2.6. Development the mathematical model

2.6.1. Creating a random tuple from the sample

Let n be the multidimensional random variant representation (X_1, X_2, …, X_n), (Y_1, Y_2, …, Y_n), (W_1, …, W_n) and (Z_1, Z_2, …, Z_n), which represent values for Pb, F, Cn and As respectively. These multidimensional variables are taken from the set of all available random sizes n that can be drawn from the Sissili data collection. This defines the probability distribution as X for X_i, Y for Y_i, W for W_i and Z for Z_i [60–65].

All summable quantities in the sample are considered here as representations of probable values (tuple), over all representations of the multidimensional random variant named n [60,62,66–69], as shown in Equation (7):

$$\overline{x}=\frac{1}{n}\sum_{n=1}^{n}x_1,\overline{y}=\frac{1}{n}\sum_{n=1}^{n}y_1,\overline{w}=\frac{1}{n}\sum_{n=1}^{n}w_1 \text{ and } \overline{z}=\frac{1}{n}\sum_{n=1}^{n}z_1 \tag{7}$$

$\overline{x}$, $\overline{w}$ and $\overline{z}$ are the realizations, in the samples considered, of the average empirical random variables defined respectively by Ref. [17]. Given Equations (8) and (9):

$$\overline{X}=\frac{1}{n}\sum_{n=1}^{n}X_1,\overline{Y}=\frac{1}{n}\sum_{n=1}^{n}Y_1,\overline{W}=\frac{1}{n}\sum_{n=1}^{n}W_1 \text{ and } \overline{Z}=\frac{1}{n}\sum_{n=1}^{n}Z_1 \tag{8}$$

$$S_{n,x}^2=\frac{1}{n}\sum_{n=1}^{n}(x_i-\overline{x})^2,S_{n,y}^2=\frac{1}{n}\sum_{n=1}^{n}(y_i-\overline{y})^2,S_{n,w}^2=\frac{1}{n}\sum_{n=1}^{n}(w_i-\overline{w})^2 \text{and } S_{n,z}^2=\frac{1}{n}\sum_{n=1}^{n}(z_i-\overline{z})^2 \tag{9}$$

are the realizations, in the considered samples, of the empirical variances of the random variables defined by Equation (10):

$$S_{n,x}^2=\frac{1}{n}\sum_{n=1}^{n}(X_i-\overline{X})^2,S_{n,y}^2=\frac{1}{n}\sum_{n=1}^{n}(Y_i-\overline{Y})^2,S_{n,w}^2=\frac{1}{n}\sum_{n=1}^{n}(W_i-\overline{W})^2 \text{and } S_{n,z}^2=\frac{1}{n}\sum_{n=1}^{n}(Z_i-\overline{Z})^2 \tag{10}$$

2.6.2. Determination of the average pollution for X defined

Consider the variable X, σ_x which is already defined.

If X ⇝ N (μ_x, σ_x), so $\forall$ i ∈ {1, …, n}, X_i ⇝ N (μ_x, σ_x), and $\overline{X}$ ⇝ N (μ x, $\frac{\sigma_x}{\sqrt{n}}$).

If there is a risk named $\alpha = 0.05$, the proportional distribution matrix of centred values produces a result $u_{\alpha/2} = 1645$ for which [20], defined as in Equations (11)–(14):

$$P\left[-u_{\alpha/2}\le\frac{\overline{X}-\mu_x}{\frac{\sigma_x}{\sqrt{n}}}\le u_{\alpha/2}\right]=1-\alpha \tag{11}$$

$$\text{We then have } P\left[-u_{\alpha/2}\ \frac{\sigma_x}{\sqrt{n}}\le\overline{X}-\mu_x\le u_{\alpha/2}\ \frac{\sigma_x}{\sqrt{n}}\right]=1-\alpha \tag{12}$$

$$\text{Let } P\left[\overline{X}\text{-}u_{\alpha/2}\ \frac{\sigma_x}{\sqrt{n}}\ \mu_x\le\overline{X}+u_{\alpha/2}\ \frac{\sigma_x}{\sqrt{n}}\right]=1-\alpha \tag{13}$$

$$\text{We did find two v.a : } T_1(X_1,X_2,\ldots,X_n)=\overline{X}-u_{\alpha/2}\ \frac{\sigma_x}{\sqrt{n}} \text{ et } T_2(X_1,X_2,\ldots,X_n)=\overline{X}+u_{\alpha/2}\frac{\sigma_x}{\sqrt{n}} \tag{14}$$

2.6.3. Determination of the ranges of the number of polluted boreholes in case X undefined

The variable μ_x is undetermined. Let us consider $S_{57,x}^2$ as an estimator of σ^2.

If - $\overline{X}$ ⇝ N (μ_x, σ_x) as shown in Equation (15), then

$$\frac{(n-1)s_{57,x}^2}{\sigma^2}=\frac{\sum_{i=1}^{n}(Xi-\overline{X})^2}{\sigma^2}\rightsquigarrow x_{(57)}^2 \tag{15}$$

For an (alpha) hazard $\alpha = 0.05$, the Chi-square matrix with 57 factors gives z_1 and z_2 as shown in Equation (16):

$$P\left[z_1\le\frac{(n-1)S_{n-1,x}^2}{\sigma^2}\le z_2\right]=1-\alpha \tag{16}$$

Since the interval [z_1, z_2] is not uniform and depends closely on the indeterminate variable α_1 and α_2 such that $\alpha_1 + \alpha_2 = \alpha$. But in

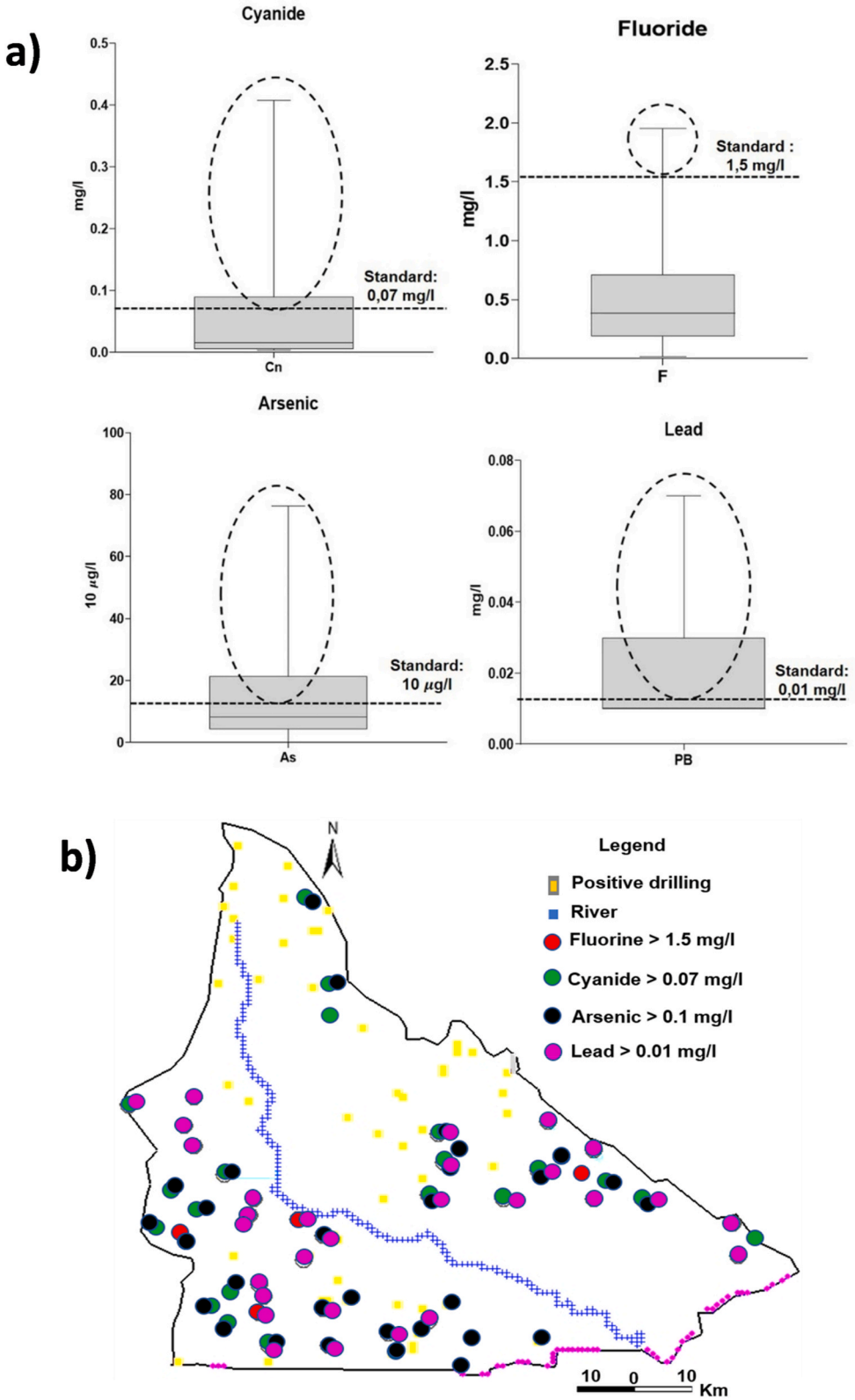

Fig. 6. Distribution of micropollutants and water extraction points for polluted boreholes. **a**: Box plot showing the distribution of micropollutants. **b**: water extraction points for polluted drillings.

this practical case we will consider $\alpha_1 = \alpha_2 = \alpha/2$ [57].

2.6.4. Determination of mean pollution for X normally distributed and σ undefined

X has a normal distribution, σ x which is not defined. For this purpose, we consider the following variable given in Equation (17):

$$T_x = \frac{\overline{X} - \mu_x}{\frac{S_{n-1,x}}{\sqrt{n}}} \tag{17}$$

With $S_{n-1,x} = \frac{57}{58} * S_{n,x}$

following a 58 factor estimation rule. Given a risk named $\alpha = 0.05$, the proportional distribution matrix of the 58 centred values gives a result $t_{\alpha/2} = 1{,}669$, defined as in Equations (18) and (19) for which [17,58]:

$$P\left[-t_{\alpha/2} \leq \frac{\overline{x} - \mu}{\frac{S_{n-1}}{\sqrt{n}}} \leq t_{\alpha/2}\right] = 1 - \alpha \tag{18}$$

$$\text{Let } P\left[\overline{X}\text{-}t_{\alpha/2}\ \frac{S_{n-1}}{\sqrt{n}} \leq \mu_x \leq \overline{X} + t_{\alpha/2}\frac{S_{n-1}}{\sqrt{n}}\right] = 1 - \alpha \tag{19}$$

2.6.5. Determination of the ranges of the number of polluted boreholes in case X is defined

X has a normal distribution, σ_x which is defined.

If $X \rightsquigarrow N(\mu_x, \sigma_x)$, so $\forall i \in \{1, \ldots, n\}$, $X_i \rightsquigarrow N(\mu_x, \sigma_x)$ and $X \rightsquigarrow N(\mu_x, \frac{\sigma_x}{\sqrt{n}})$.

If there is a risk named $\alpha = 0.05$, the proportional distribution matrix of centred values produces a result $\mu_{\alpha/2} = 1{,}645$, defined as in Equations (20), (21), (22) and (23), for which [17]:

$$P\left[-u_{\alpha/2} \leq \frac{\overline{x}\text{-}\mu_x}{\frac{\sigma}{\sqrt{n}}} \leq u_{\alpha/2}\right] = 1 - \alpha \tag{20}$$

$$\text{We then have} \quad P\left[-u_{\alpha/2}\ \frac{\sigma_x}{\sqrt{n}} \leq \overline{X}\text{-}\ \mu_x \leq u_{\alpha/2}\ \frac{\sigma_x}{\sqrt{n}}\right] = 1 - \alpha \tag{21}$$

$$\text{Let} \quad P\left[\overline{X}\text{-}u_{\alpha/2}\ \frac{\sigma_x}{\sqrt{n}} \leq \mu_x \leq \overline{X} + u_{\alpha/2}\ \frac{\sigma_x}{\sqrt{n}}\right] = 1 - \alpha \tag{22}$$

$$\text{We did find two v.a : } T_1\ (X_1, X_2, \ldots, X_n) = \overline{X}\text{-}u_{\alpha/2}\frac{\sigma_x}{\sqrt{n}} \text{ et } T_2\ (X_1, X_2, \ldots, X_n) = \overline{X} + u_{\alpha/2}\frac{\sigma_x}{\sqrt{n}} \tag{23}$$

3. Results and discussion

3.1. Sampling and analysis results

The results (Fig. 6a and b) of the analyses show that concentrations of F are within the range of 0.01 mg/l to 1.95 mg/l, whereas the national standards in Burkina Faso advise a limit of 1.5 mg/l I should be noted that 2 boreholes are over this limit, namely the village of Koumbila (south-western) with a concentration of 1.65 mg/l and the district of 5 of Léo (south-western) with a concentration of 1.95 mg/l. This can further be explained by an intrusion of granites in the local geology. Moreover, these boreholes are located in agricultural areas, which suggests that they are the result of dissolution of minerals such as fluorite (CaF_2), cryolite (Na_3AlF_6), fluo-apatite ($Ca_5F(PO_4)$) and micas present in the rocks.

Cn results show concentrations within the range of 0.001 mg/l to 0.4 mg/l, with a national limit set to 0.07 mg/l. Overall, 19 boreholes are above this standard and are located in areas where traditional gold panning activities are widespread (citer les zones). We also note the presence of non-regulatory rubbish dumps, as well as farms [6] mention massive deaths of cattle due to contamination of surface water in the locality of Boromo (south-western), therefore it is important to see the evolution of this contamination in the future as the subsoil is composed essentially of rocks rich in Arsenic.

Arsenic concentrations vary within the range of 0.00001 mg/l to 0.41 mg/l, while the standard limit in Burkina Faso is of 0.01 mg/l. About 31 boreholes have values higher than this limit and are mostly located in gold panning areas or polluted areas near underground fractures. According to the national agency in charge of mining and geological studies (in French "*Bureau des Mines et de la Géologie du Burkina Faso*", BUMIGEB), different elements such as pyrite and arsenopyrite are part of the natural composition of the subsoil in Burkina Faso in different concentrations. Therefore, there might be cases where the sulphur walls are affected, resulting in the mobilisation of toxic traces in the groundwater [16]. Apart from its rock-related presence, the basic pH could also explain the high

concentrations, but also dissolved oxygen concentrations below 2 mg/l can cause a raise in the concentrations measured.

Pb concentrations vary within the range of 0.01 mg/l to 1.51 mg/l. In contrast to organic pollutants, degradation is almost impossible. The presence of Pb in its waters is the result of diffuse pollution.

3.2. Conceptual model and calibration results

In the pollutant transfer analysis, the spread of the pollutant appears to be governed by the weathering network. Since we are dealing with a discontinuous environment, only the cracks influence the direction of groundwater flow. Fig. 4 shows the weathering map distribution in the study area, from which the directions are deducted. The identification of the main corridors provides major NW-SE (Eburnian) and NE-SW directions and a minority NS and E-W (Liberian) class. There are also N60°–70°, N140°–150° directions with peaks in frequency. According to Fig. 4, through the superimposition of the boreholes on the fractures, several directions N0°–N20°, N60°–N70°, which represent negative boreholes and therefore closed joints are revealed. Joints open at the surface can however be closed at shallow depth. Others, on the other hand, have directions N90°–N100°, N120°–N130° and N160°, which represent positive boreholes and therefore open joints [31]. It has been considered that the open directions are the most capable of having a major drainage role with respect to the surrounding alterites. Preferential directions N10°–15°, N30°–35°, N185°–90° are encountered. The directions can be combined in pairs of directions N°10–20°, N°60–70°, N100°–110°.

The development of the numerical model starts with the spatial discretization of the domain. In this study, a single layer representation is adopted due to the limited availability of the data from the domain to be modelled.

In the MODFLOW design, a clear distinction should be made between active meshes, where the hydraulic head is calculated at each iteration using a pre-defined initial position, non-active meshes with nil (zero) flow, meshes with imposed potential, and meshes with user-imposed head. In the Sissili sub-catchment, there is no physical boundary, therefore we used the imposed potential as a boundary condition and then superimposed it on the piezometric map to obtain the flow values at the boundary contours. The imposed head boundaries correspond to the granitic formations.

In the steady-state simulation, based on calibration using 2019 data, four hydraulic conductivity zones are defined. The recharge value that allowed the optimal fit to be achieved was 0.54 mm/d, i.e. 5% of annual precipitation. Given this low value, contamination is likely to occur very slowly over the years due to the longer residence time. The statistical results of the consistent values of the manual calibration method are presented in Table 1, which indicate an optimal RMSE of 0.98 m, deemed to be acceptable since it is less than the uncertainty of the topographic data used in this study.

Further, the water balance has been assessed, therefore enabling the flows transiting through the aquifer to be quantified (in Table 2), to represent the overall balance of the aquifer. Also the relative percentage of bias between water inflow and outflow is 0.000035%, which is less than the 0.1% recommended by Ref. [49].

After an acceptable calibration of the model follows the validation step, which is carried out in this study through the simulation of the 2020 values. The results are presented in Table 3. The analysis shows that the values are approximately similar, therefore the calibrated model can be considered satisfactory.

A sensitivity test is performed after the model has been calibrated and validated. This is carried out in order to assess the parameters which control the groundwater flow dynamics through the effect of the modification of hydraulic conductivity and recharge in the model.

Regarding groundwater recharge, a 30% decrease or increase results in a decrease in the simulated head. However, this has little impact on the simulated head, while the mass balance remains stable. In fact, the results of such tests show that the model is hardly sensitive to changes in the head. It is also noted that the decrease in recharge slightly increases the deviations for certain piezometers.

Regarding conductivity, it is observed in this case that a 10% increase in hydraulic conductivity leads to a slight decrease in the simulated and observed heads. This is due to the fact that an increase in conductivity favours groundwater flow. A 10% decrease in hydraulic conductivity results in an increase of 16.37 m in the calculated head. In fact, this decrease results in a limitation of flow while maintaining higher loads. However, the RMSE therefore obtained is of 1.056 m, which is higher under the observed heads. The conductivity in some areas has an impact on the head, therefore it can be assumed that these areas control the groundwater flow from upstream due to their proximity to the Sissili River or through preferential recharge pathways. This can be explained by the fact that groundwater flow (which depends on the volume in the faults) in terms of potential is more represented in these areas.

From these results, it can be concluded that the model is more sensitive to the decrease in hydraulic conductivity. The model is therefore reliable for these variables in steady state.

Table 1
Statistical evaluation of the performance of the model calibration.

Criteria	Value
Minimum residual (m)	−1.524
Maximum residual (m)	1.136
ME (m)	−0.469
MAE (m)	0.836
R^2	0.99
RMSE (m)	0.983

Table 2
Mass balance of the calibrated model.

Designations Designation Inflow (m^3/day) Outflow (m^3/day)		
Constant costs	1129501.77	140152.91
Total	5129349.81	5129348.01
Total inputs - total outputs = 1.80		
Percentage of anomaly = $3.5008114.10^{-5}$		

Table 3
Validation test statistics.

Designations	Calibrated model	Validated model
Minimum residual (m)	−1524	−1998
Maximum residual (m)	1136	1660
AE (m)	−0.469	−0.202
MAE (m)	0.836	0.920
R^2	0.99	0.973
RMSE	0.983	1190

3.3. Model simulations

After having calibrated the GMS and developed the MT3D code, the different concentrations for the four substances in the water of the Sissili sub-catchment. To do this, we assign concentration levels to the different pollutants determined in the study area and corresponding to the concentrations obtained by the 2012 survey. Here the pumping rate is constant. This allows us to reproduce the real conditions in 2012 in order to determine the current fate of the pollutant in 50 years as shown in Fig. 7, whereas for the other cells the concentration is nil.

The pollution converges in the direction of the flow downstream of the borehole in abundance over time. This convergence is due to the dispersion coefficient. The dispersion elements thus play a dominant role in the modification of the contaminant. It would thus be much more relevant to carry out field measurements, such as tracer tests, to further constrain the model, and thus reform its predictive properties. Fig. 7 also shows that the distribution of recharge results in a lower concentration of Pb and Cn in the municipalities in the center of the study area. The influence of the flows from the catchment is noticeable, with a decrease in concentrations in some places,

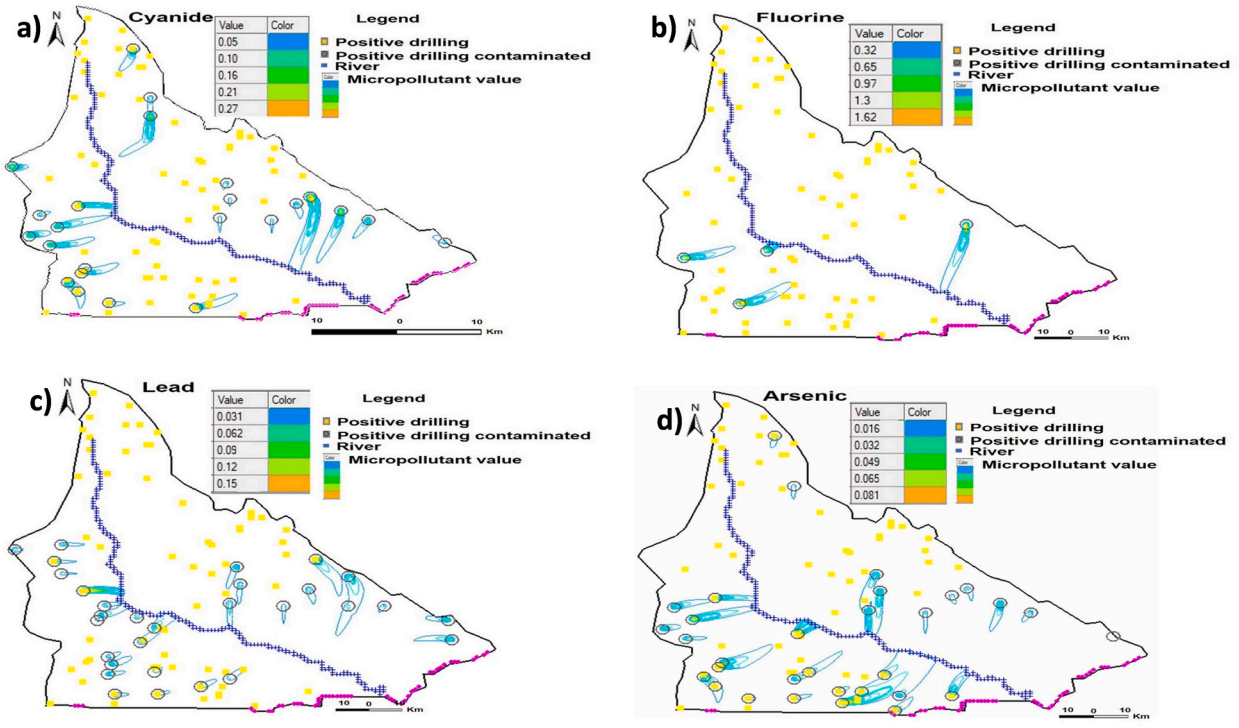

Fig. 7. Evolution of the concentration over 50 years of the four pollutants. a) Cyanide. b) Fluorine. c) Lead. d) Arsenic.

since the mass flow imposed on the external boundaries is nil. Also, for Cn, Pb and F, a dilution phenomenon is observed for some boreholes, and shows us a fairly slow deterioration in water quality for Pb, which extends over 22 km, Cn over a distance of 2–16 km and F which extends from 4 to 10 km. The As also degrades fairly quickly, extending from 3 to 11 km due to the geology. This would suggest that in these areas the water table is recharged by the river. This deduction is verified in the simulation, for example for Pb we see that only one borehole converges. While the concentration of this borehole is lower than the other concentration values. However, there are some areas that appears to be rapidly more affected than others, which may be the difference between the concentration trends simulated at the different boreholes. This is due to the unsaturated zone which is the key element for the transfer, especially for the delay or acceleration of the pollutant dispersion. It multiplies the pollution more than in the surface aquifer, as well as the position considered in the sub-catchment. If the unsaturated zone is thick, the flow is slow, hence the system reacts to the change in flow.

Generally, the transfer model shows that shallow wells are more polluted than deep wells. In the long term, all the boreholes that tap the alterites have excess micropollutants, high above the national standards. Although the pollution of fractured aquifers is conditioned by the quality of the water in the upper layer, this does not necessarily mean that these aquifers are polluted. In fact, the passage of pollution from the alterites to the fractured rock is conditioned by the difference in hydraulic head, conductivity and the thickness of the alteration. These factors enable us to define the vertical percolation velocity according to Darcy's law. Added to this is the dilution of the contamination in relation to the stock of water confined in the aquifer. This modeling shows that over the next 50 years and beyond, there are potentially dangerous areas for drilling if nothing is done in terms of mitigation measures. Especially since decontamination is very costly [31]. The simulation considered the values of the 2012 sample, so the consideration is not underestimated, but it should also be noted that the diffusion rate of the contaminant may be conservative due to rock-water interactions. But for a deeper understanding, a simulation in transient regime is recommended and is in perspective.

3.4. Mathematical model: estimation of the different means Equation (24)

$\theta_x = E[X] = \mu_x$, $\theta y = E[Y] = \mu_y$, $\theta z = E[Z] = \mu_z$, $n = 58$.
$\overline{x} = \frac{1}{n}\sum_{n=1}^{n} x_1$, average of the sampled values, is an assessment of μ_x.
$\overline{X} = \frac{1}{n}\sum_{n=1}^{n} X_1$, random variable with "mean empirical", is an evaluator of μ_x.

$$\overline{y} = \frac{1}{n}\sum_{n=1}^{n} y_1, \text{ mean of the values found in the sample, is an evaluator of } \mu_y. \tag{24}$$

$\overline{Y} = \frac{1}{n}\sum_{n=1}^{n} Y_1$, "empirical mean" random variable, is an estimator of μ_y.
$\overline{z} = \frac{1}{n}\sum_{n=1}^{n} z_1$, average of the sampled values, is an assessment of μ_z.
$\overline{Z} = \frac{1}{n}\sum_{n=1}^{n} Z_1$, random variable with "mean empirical", is an evaluator of μz (see Table 4).
The characteristics of the selection of a mean are as follows
$E[\overline{X}] = E(X) = 0.02000000 = \mu_x$
$E[\overline{Y}] = E(Y) = 0.40000000 = \mu_y$
$E[\overline{W}] = E(W) = 0.06421050 = \mu_w$
$E[\overline{Z}] = E(Z) = 15.3468421 = \mu_z$

3.5. Determination of the interval limit

Let X, Y, W and Z are a population defined random variable with a mean μ_x, μ_y, μ_w and μ_z, of variance σ_x^2 σ_y^2, σ_{xw}^2 and σ_z^2. We have 58 sampling, for a rational use of the inferential statistical standard, we need to define the various means as those of the contamination we seek to determine. Often also in certain contexts, the laws X, Y, W and Z are known or unknown. In this case we have two assumptions.

3.5.1. Limit interval of means (μ is defined)

Suppose Equation (25), $\overline{X}$ is the forecast of μ: $E[\overline{X}] = E[X] = \mu$

$$\text{and var } (\overline{X}) = \frac{Var\,(X)}{n} = \frac{\sigma^2}{n} \tag{25}$$

Table 4
Summary table of parameters.

	X	Y	W	Z
E [.]	0.3000000	0.50000000	0.06421050	15.3468421
V (.)	0.0547963	0.15632838	0.00980338	232.196076
σ (.)	0.02340861	0.3953838	0.09901200	15.2379813
max (.)	1.510000	1.9500000	0.41000000	76.4200000
min (.)	0.060000	0.0100000	0.00000100	2.76000000
Σ	16.930000	28.260000	3.600000	874.770000

Case 1. Assessment of mean contamination

Estimated average contamination of Pb, F, Cn and As

X, Y, W and Z is normal distribution, σ_x, σ_y, σ_w, and σ_z is known, as shown in Equation (26).

If X ⇝ N (μ_x, σ_x), so $\forall$ Xi ∈ {1, …,n}, X_i ⇝ N (μ_x, σ_x) and $\overline{X}$ ⇝ N (μ_x, $\frac{\sigma_x}{\sqrt{n}}$).

$$\text{If } Y \rightsquigarrow N\left(\mu_y,\sigma_y\right), \text{so } \forall i \in \{1,\ldots,n\}, Y_i \rightsquigarrow N\left(\mu_y,\sigma_y\right) \text{ and } \overline{Y} \rightsquigarrow N\left(\mu_y,\frac{\sigma_y}{\sqrt{n}}\right). \tag{26}$$

If W ⇝ N (μ_w, σ_w), so $\forall$ i ∈ {1, …,n}, W_i ⇝ N (μ_w, σ_w) and $\overline{W}$ ⇝ N (μ_w, $\frac{\sigma_w}{\sqrt{n}}$).

If Z ⇝ N (μ_z, σ_z), so $\forall$ i ∈ {1, …,n}, Z_i ⇝ N (μ_z, σ_z) and $\overline{Z}$ ⇝ N (μ_z, $\frac{\sigma_z}{\sqrt{n}}$).

In the case of a risk of the variable $\alpha = 0.05$, the centred reduced probability law allows us to obtain a figure $\mu_{\alpha/2} = 1645$ Relation 5 makes it possible to obtain for this specific case X (the same reasoning is applied to the other variable Y, W and Z).

We concluded that in the Sissili sub-catchment, the degree of groundwater contamination is understood as shown in the following (Table 5) within the probable error tolerance of 5%. In summary, considering that σ is well known and that X, Y, W and Z follow a weak normal.

Case 2. Assessment of mean contamination

Estimated average contamination of lead, fluorine, cyanide and arsenic

X, Y, W and Z is normal distribution, σ_x, σ_y, σ_w, and σ_z is indeterminate. To do this, we must consider (as an example for X), defined as in Equations (27)–(29).

$$T_x = \frac{\overline{X}_- \mu_x}{\frac{S_{n-1,x}}{\sqrt{n}}} \tag{27}$$

0.02 00000 with $S_{57,x} = \frac{57}{58} \times S_{58,x} = 0.40$.which follows a Student law with 58 degrees of freedom. In the case of a risk of the variable α = 0.05, the probability law allows us to obtain a figure 58 degrees of freedom gives $t_{\alpha/2} = 2.0086$ given as

$$P\left[-t_{\alpha/2} \leq \frac{\overline{X}-\mu}{\frac{S_{n-1,x}}{\sqrt{n}}} \leq t_{\alpha/2}\right] = 1 - \alpha \tag{28}$$

$$\text{Let } P\left[\overline{X}-t_{\alpha/2}\frac{S_{n-1,x}}{\sqrt{n}} \leq \mu_x \leq \overline{X}+t_{\alpha/2}\frac{S_{n-1,x}}{\sqrt{n}}\right] = 0,95 \tag{29}$$

It is assumed that the interval (1–0.05) × 100 is more likely to be in the interval of the mean described in the following (Table 6) for the variables σ_x, σ_y, σ_w, and σ_z.

As long as σ_x, σ_y, σ_w, and σ_z is defined and X, Y, W and Z follows a probability distribution.

Case 3. Assessment of mean contamination

Estimated average contamination of Pb, F, Cn and As

X is an undefined element distribution, and n large (n = 58).

The assumptions made for the limits of probability are true, so it follows that X ⇝ N (μ_x, $\frac{\sigma_x}{\sqrt{58}}$)

- In the case where σ is defined, we are brought back to the first case.
- If σ undefined, it is necessary to assume of normality of the distribution of X in order to consider the variant of Student. Nevertheless, n being large, the regulation on samples can be approximated by a centred reduced probability distribution and we find a similarity to the 1st case (where we consider σ by $S_{n-1,}$).

Let X, Y, W and Z are a probability value derived from the sample, with average μ_x, μ_y, μ_w and μ_z, of variance σ_x^2, σ_y^2, σ_w^2, and σ_z^2. We have 58 samples, we assume that the different averages are the averages of another sample in order to consider the laws of inferential statistics. There are several situations that present themselves to us. Either the distributions of X, Y, W and Z are defined or not. This leads us to the following assumptions.

Table 5
Interval for degree of groundwater contamination.

	T_1	T_2
X	0.25	0.34
Y	0.41	0.58
W	0.042	0.85
Z	12.05	18.63

Table 6
The range of the mean.

	T_1	T_2
X	0.23	0.35
Y	0.39	0.60
W	0.038	0.090
Z	11.25	19.44

3.5.2. *Limits of the confidence interval of a mean (μ undefined)*

Let Equation (30), us consider $\overline{X}$ is the forecast of μ: E $[\overline{X}]$ = E $[X]$ = μ

$$\text{and var } (\overline{X}) = \frac{Var\ (X)}{n} = \frac{\sigma^2}{n} \tag{30}$$

Case 1. Estimated average contamination of Pb, F, Cn and As

X, Y, W and Z is normal distribution, σ_x, σ_y, σ_w, and σ_z is known, as shown in Equation (31).

If X ⇝ N (μ_x, σ_x), so ∀ Xi ∈ {1, …,n}, X_i ⇝ N (μ_x, σ_x) and $\overline{X}$ ⇝ N (μ_x, $\frac{\sigma_x}{\sqrt{n}}$).

$$\text{If } Y \rightsquigarrow N\left(\mu_y,\sigma_y\right), \text{so } \forall\, i \in \{1,\ldots,n\}, Y_i \rightsquigarrow N\left(\mu_y,\sigma_y\right) \text{ and } \overline{Y} \rightsquigarrow N\left(\mu_y, \frac{\sigma_y}{\sqrt{n}}\right). \tag{31}$$

If W ⇝ N (μ_w, σ_w), so ∀ i ∈ {1, …,n}, W_i ⇝ N (μ_w, σ_w) and $\overline{W}$ ⇝ N (μ_w, $\frac{\sigma_w}{\sqrt{n}}$).

If Z ⇝ N (μ_z, σ_z), so ∀ i ∈ {1, …,n}, Z_i ⇝ N (μ_z, σ_z) and $\overline{Z}$ ⇝ N (μ_z, $\frac{\sigma_z}{\sqrt{n}}$).

In the case of a risk of the variable α = 0.05, the centred reduced probability law allows us to obtain a figure $\mu_{\alpha/2} = 1645$. Therefore, relation 5 makes it possible to obtain for this specific case X (the same reasoning is applied to the other variable Y, W and Z), defined as in Equations (32) and (33).

$$\text{We then have } P\left[\overline{X}\text{-}u_{\alpha/2}\ \frac{\sigma_x}{\sqrt{n}} \le \mu_x \le \overline{X}+u_{\alpha/2}\ \frac{\sigma_x}{\sqrt{n}}\right] = 1 - \alpha \tag{32}$$

by application of relation 6 we did find two v.a:

$$T_1\ (X_1,X_2,\ldots,X_n) = \overline{X}\text{-}u_{\alpha/2}\frac{\sigma_x}{\sqrt{n}} \text{ et } T_2\ (X_1,X_2,\ldots,X_n) = \overline{X} + u_{\alpha/2}\frac{\sigma_x}{\sqrt{n}} \tag{33}$$

The results show that in Sissili, the daily pollution interval is comprised according to the values in Table 7, with an assumed error of 5%. Indeed, if σ_x, σ_y, σ_w, and σ_z is defined and X, Y, W and Z is towards the normal.

Case 2. Estimated average contamination of Pb, F, Cn and As

X, Y, W and Z is normal distribution, σ_x, σ_y, σ_w, and σ_z is undefined as in Equations (34) and (35). To do this, let's consider:

$$T_x = \frac{\overline{X}_{-}\mu_x}{\frac{S_{n-1,x}}{\sqrt{n}}} \tag{34}$$

$$\text{with } S_{57,x} = \frac{57}{58} \times S_{58,x} = 0.40. \tag{35}$$

which follows a Student law with 58 degrees of freedom. In the case of a risk of the variable α = 0.05, the probability law allows us to obtain a figure 58 degrees of freedom gives $t_{\alpha/2} = 2.0086$ given as in Equations (36) and (37)

$$P\left[\text{-}t_{\alpha/2} \le \frac{\overline{X}\text{-}\mu}{\frac{S_{n-1,X}}{\sqrt{n}}} \le t_{\alpha/2}\right] = 1 - \alpha \tag{36}$$

Table 7
Daily pollution intervals.

	T_1	T_2
X	0.25	0.34
Y	0.41	0.58
W	0.042	0.85
Z	12.05	18.63

$$\text{Let } P\left[\overline{X}\text{-}t_{\alpha/2}\ \frac{S_{n\text{-}1,x}}{\sqrt{n}} \le \mu_x \le \overline{X} + t_{\alpha/2}\frac{S_{n\text{-}1,x}}{\sqrt{n}}\right] = 0,95 \tag{37}$$

It is assumed that the interval (1–0.05) × 100 is more likely to be in the interval of the mean described in the following (Table 8) for the variables σ_x, σ_y, σ_w, and σ_z.

In another case, let us assume that σ_x, σ_y, σ_w, and σ_z is undefined and that X, Y, W and Z converges to normal.

Case 3. Z is an undefined element distribution, and n is large (n = 58).

The assumptions made for the limits of probability are true, so it follows that $Z \rightsquigarrow N\left(\mu_z, \frac{\sigma_z}{\sqrt{58}}\right)$

- In the case where σ is defined, we are brought back to the first case.
- If σ undefined, it is necessary to make the postulate on the normality of the distribution of X to be able to use the t-Student variable. However, as long as N is large, we limit ourselves to the reduced normal distribution and we find ourselves in the same order as the first case. We estimate σ by $S_{n-1,}$ without any limit in the assumption of normality of Z.

3.5.3. Limit of the reliability interval of a variance

To determine the variance of the number of Pb, F, Cn and As polluted boreholes by 0.95 reliability interval, defined as in Equations (38) and (39) we assume:

μ_x unknown. We take $S^2_{57,x}$ as estimator of σ^2. If $\overline{X} \rightsquigarrow N\ (\mu_x, \sigma_x)$.

$$\mu_y \text{ unknown. We take } S^2_{57,y} \text{ as estimator of } \sigma^2. \text{ If } \overline{Y} \rightsquigarrow N\left(\mu_y, \sigma_y\right). \tag{38}$$

μ_w is undefined. We take $S^2_{57,w}$ as an evaluator of σ^2. If $\overline{W} \rightsquigarrow N\ (\mu_w, \sigma_w)$.

μ_z is undefined. We take $S^2_{57,z}$ as an evaluator of σ^2. If $\overline{Z} \rightsquigarrow N\ (\mu_z, \sigma_z)$.

Example for X (the same reasoning is e applied to the other variable Y, W and Z)

$$\frac{(n-1)s^2_{n-1,x}}{\sigma^2_x} = \frac{\sum_{i=1}^{58}(Xi - \overline{X})^2}{\sigma^2_x} \rightsquigarrow x^2_{(57)} \tag{39}$$

In the case of a risk of the variable α = 0.05, the chi-square with 58 samples gives z1 and z2 given as in Equation (40):

$$P\left[z_1 \le \frac{(n-1)S^2_{n-1,x}}{\sigma^2_x} \le z_2\right] = 1-\alpha \tag{40}$$

As the interval [z1, z2] is not unique, and they are related to risks α1 and α2 allowed outside the, defined as in Equations (41), (42), (43) and (44).

Indeed z1 is such that

$$P\left(\frac{57xs^2_{57,x}}{\sigma^2_x} < z_1\right) = a_1 \tag{41}$$

$$z2 \text{ is given by } P\left(\frac{57xs^2_{57,x}}{\sigma^2_x} < z_2\right) = a_2 \tag{42}$$

with α1 + α2 = α.

For n > 30 the chi-2 distribution is close to normal distribution N (58, $\sqrt{58}$).

$$\frac{z_2 - 58}{\sqrt{58}} = \frac{0,68 + 0,69}{2} \text{ then } z1 = 63,21. \tag{43}$$

using the same process, we have z1 = 58–2.81 × $\sqrt{58}$ from where z 2 = 36.59

If we consider symmetric risks α1 = α2 = α/2, we get (1–0.05) × 100 chance out of 100

Table 8
Ranges of mean values.

	T_1	T_2
X	0.23	0.35
Y	0.39	0.60
W	0.038	0.090
Z	11.25	19.44

$$\frac{\sum_{i=1}^{58}(Xi-\overline{X})^2}{z_2},\frac{\sum_{i=1}^{58}(Xi-\overline{X})^2}{z_1}=\frac{58*0.055}{63.21},\frac{58*0.055}{36.59}=[0.05;0.08] \tag{44}$$

recovered variance σ_x^2. We choose $S_{57,x}^2=\frac{1}{n}\sum_{i=1}^{58}(Xi-\overline{X})^2$ as an evaluator of σ^2. If $\overline{X}$ ⇝ N (μ, σ), we have as shown in Equation (45)

$$\frac{58\ *\ s_{58,x}^2}{\sigma_x^2}=\frac{\sum_{i=1}^{58}(Xi-\overline{X})^2}{z_2}\rightsquigarrow x_{(58)}^2 \tag{45}$$

because the Xi are autonomous entities and of the same law N (μ_x, σ_x). In the case of a risk of the variable α, the Chi-2 with n dimensions establishes a value between 36.59 and 63.21 given as $P\left[z_1\le\frac{58*S_{n-1,x}^2}{\sigma_x^2}\le z_2\right]=0.95$ hence the limit of the reliability interval of the risk 0.05 for σ_x, σ_y, σ_w, and σ_z is defined in Table 9:

Table 10 summaries the various forecasts obtained from the modelling step.

- I_1 tolerance interval at 95% confidence assuming that X follows a normal distribution with known variance (σ).
- I_2 reliability thresholds at 95% reliability assuming that X follows a normal distribution with unknown variance (σ).
- I_σ represents the tolerance limit of the variance with a 95% reliability threshold.

From all the above we find that all concentration averages verify the mathematical models. The techniques used in the two cases (cases 1 and 2) produce intervals I1 and I2 that are very close altogether.

In Table 11, to validate the data simulated over 50 years GMS, we have multiplied the bounds of the different intervals by the longitudinal dispersion coefficient.

We find that the value of the Pb concentration at 50 years does not verify the intervals of the error model. Whereas for the other micropollutants (F, Cn and As) the mathematical model confirms the simulation results with GMS. However, there are areas that are quickly more affected than others. It is due to the unsaturated zone which is the key element, in particular for the delay or the acceleration of the pollutant.

The Pb concentration at 50 years is 0.17. It does not check the two intervals I1 [0.50; 0.68] and I2 [0.46, 0.70]. This is due to Pb dilution phenomena observed in certain boreholes. This suggests that the water table is fed by the river. This deduction is verified by the fact that at the level of the simulation only one borehole converges in terms of pollution. The distribution of the recharge results in a lower concentration in the center of the catchment. It has been demonstrated in previous works that when the geological formation is acidic, the water is aggressive and can release metals. However, when the rock is of a basic nature like our case, the corrosive action depends on its content of ions of this metal, but also on its content of other ions capable of entering into oxidation reduction reactions [8,9].

F has a concentration value at 50 years is 0.97. It checks the two intervals I1 [0.82; 1.16] and I2 [0.78, 1.20]. Its presence throughout the Sissili sub-basin can be explained by granite intrusion in the local lithology [5]. F in water arises primarily from the dissolution of natural minerals found in rocks and soils with which the water reacts. Fluorite (CaF_2), cryolite (Na_3AlF_6), fluorapatite ($Ca_5F(PO_4)$) and micas are the main minerals which contain it [70].

As has a 50-year concentration value of 37.93. It checks the two intervals I1 [24.10; 37.26] and I2 [23.86; 37.50]. It should be remembered that As is normally present in formations at varying concentrations in Burkina Faso [11]. Reports relating to the As health-related problem do not identify precisely the nature of the rock formations, although it is established that the Birrimean furrows are the source of the high levels of As in groundwater, found in many numerous boreholes in the sub-catchment. It is through the covering of paleo-fluviatiles that the mechanisms for transporting vertical flows towards the formations are organized. On the other hand, the appearance or presence of any harmful elements in the groundwater is due to the fact that the sulphide walls are affected [24]. The water consumed by the population is drinkable at the level of the boreholes where a low rate of contamination is noted compared to the water that is linked to the geological formation where arsenopyrite appears [24,71].

We find that the value of the Pb concentration at 50-years is 0.17. It does not check the two intervals I1 and I2. This is due to Pb dilution phenomena in certain boreholes. This suggests that the water table is fed by the river. This deduction is verified by the fact that at the level of the simulation only one borehole converges in terms of pollution. The distribution of the recharge results in a lower concentration in the center of the catchment.

We note that for the other micropollutants (F, Cn and As), the mathematical model confirms the simulation results with GMS. However, there are areas that are quickly more affected than others. It is due to the unsaturated zone which is the key element, especially for the delay or the acceleration of the pollutant.

4. Conclusions

This study revealed contamination and the progression of pollutant transfer, while establishing the relationship between infiltration and point source pollution in a discontinuous environment. The results of this study show an evolution of the contamination for certain boreholes. While for others there is a dilution or a lack of evolution. This evolution identifies a zone of deterioration in groundwater quality ranging from 2 to 22 km over 50 years. The concentration of pollutants is increased in superficial area as well as

Table 9
Reliability intervals of the risk.

	reliability interval
X	[0.05; 0.08]
Y	[0.02; 0.03]
W	[0.08; 0.14]
Z	[19.97; 24.14].

Table 10
Modelling forecasts.

	E [.]	*V (.)*	σ (.)	I_1	I_2	I_σ
X	0.3000000	0.0547963	0.0234086	[0.25; 0.34]	[0.23;0.35]	[0.02; 0.03]
Y	0.50000000	0.1563283	0.3953838	[0.41; 0.58]	[0.39;0.60]	[0.35; 0.61]
W	0.06421050	0.0098033	0.0990120	[0.042; 0.058]	[0.04; 0.08]	[0.08; 0.14]
Z	15.3468421	232.19607	15.237981	[12.05; 18.63]	[11.93; 18.75]	[13.97; 24.14]

Table 11
Data with the longitudinal dispersion coefficient.

	E [.]	*V (.)*	$I_1 * D_L$	$I_2 * D_L$
X	0.1726273692	0.05479630	[0.50; 0.68]	[0.46;0.70]
Y	0.9748370000	0.15632838	[0.82; 1.16]	[0.78;1.20]
W	0.1200075384	0.00980338	[0.084; 0.116]	[0.08; 0.16]
Z	37.936923076	232.196076	[24.10; 37.26]	[23.86; 37.50]

on its considered position. If the unsaturated zone is large, the rate of contamination is slow, therefore the system reacts to the change.

The use of inferential statistical techniques allowed us to develop confidence intervals at 5%. This helped in evaluating the parameters provided by the Groundwater Modelling Software (GMS) to assess their effectiveness. A convergence between the results of the mathematical modelling and the data provided by GMS is achieved. However, one of the limitations of this work was that the product of the limits of the tolerance intervals for the standard deviation by the longitudinal dispersion coefficient did not verify the results of GMS. The lack of data helped in using an inverse approach for the achievement of a steady state modelling in GMS. We recommend a transient simulation in order to develop an optimal prediction model, which considers the evolution over time. In this line of thought, the Proton Magnetic Resonance (PMR) measurements should be undertaken, which will allow the validation of the pumping tests results as well as the coupling between the transmissivity obtained from the pumping tests and the PMR results. One should also consider improving the monitoring through the piezometer network during high and low water periods. The development of a new piezometric map of the alterites water table will allow the delimitation of areas sensitive to pollution. This further heightens the need to improve the distribution of piezometric observers especially in the central and south-eastern parts of our catchment. Finally, the results of this modelling are a valuable to contribute to decision-making especially for the preservation of natural resources and sustainable management and monitoring of groundwater resources.

Data availability statement

The data associated with this study has not been deposited into a publicly available repository. All the data produced in this study will be made available upon request.

CRediT authorship contribution statement

Moussa Diagne Faye: Writing - original draft, Validation, Supervision, Software, Resources, Project administration, Methodology, Investigation, Data curation, Conceptualization. **Vini Yves Bernadin Loyara:** Writing - review & editing, Validation, Software, Resources, Methodology, Conceptualization. **Angelbert Chabi Biaou:** Writing - review & editing, Visualization, Validation, Methodology. **Roland Yonaba:** Writing - review & editing, Validation. **Mahamadou Koita:** Writing - review & editing, Validation, Funding acquisition. **Hamma Yacouba:** Writing - review & editing, Funding acquisition.

Declaration of competing interest

The authors declare that they have no known competing financial interests or personal relationships that could have appeared to influence the work reported in this paper.

Acknowledgements

The authors acknowledge the World Bank Group under the Africa Centers of Excellence for Development Impact (ACE Impact) Project [Grant D443-BF] and the Government of Burkina Faso [Credit 6388-BF] for their support.

Nomenclature

Symbol	*Name*	*Unit*
T	Transmissivity	[m^2/s]
K	Hydraulic conductivity	[m/s]
b	Thickness captured by the structure	[m]
H_c	Calculated loads	[m]
h_m	Observed loads	[m]
θ	Mass of pollution	[−]
D	Dispersion coefficient	[m^2/s]
V	Flow velocity	[m/s]
C	Concentration	[mg/l]
α_L	Longitudinal dispersivity	[m]
α_T	Transversal dispersivity	[m]
U	Velocity	[m/s]

References

[1] C. Rodríguez, B. García, C. Pinto, R. Sánchez, J. Serrano, E. Leiva, Water context in Latin America and the Caribbean: distribution, regulations and prospects for water reuse and reclamation, Water 14 (2022) 3589, https://doi.org/10.3390/w14213589.
[2] B. Dewandel, Aquifères de socle: schémas conceptuels, essais par pompage et régionalisation des propriétés hydrodynamiques, Thése de doctorat, Université de Montpellier, France, 2019.
[3] N. Courtois, P. Lachassagne, R. Wyns, R. Blanchin, F.D. Bougaïré, S. Somé, A. Tapsoba, Large-scale mapping of hard-rock aquifer properties applied to Burkina Faso, Groundwater 48 (2010) 269–283.
[4] N. Unies, Rapport sur la troisième session du Forum Urbain Mondial, 2006. Vancouver, UN-HABITAT.
[5] M.B. Kafando, M. Koïta, M. Le Coz, O.R. Yonaba, T. Fowe, C.O. Zouré, M.D. Faye, B. Leye, Use of multidisciplinary approaches for groundwater recharge mechanism characterization in basement aquifers: case of Sanon experimental catchment in Burkina Faso, Water 13 (2021) 3216.
[6] O. Bamba, S. Pelede, A. Sako, N. Kagambega, M.Y. Miningou, Impact de l'artisanat minier sur les sols d'un environnement agricole aménagé au Burkina Faso, Édité par, J. SC. 13 (2013) 1–11.
[7] R.C. Carter, A. Parker, Climate change, population trends and groundwater in Africa, Hydrol. Sci. J. 54 (2009) 676–689.
[8] M.D. Faye, M.B. Kafando, B. Sawadogo, R. Panga, S. Ouédraogo, H. Yacouba, Groundwater characteristics and quality in the cascades region of Burkina Faso, Resources 11 (2022) 61.
[9] I. Boninsenha, E.C. Mantovani, M.H. Costa, A.G. da Silva Júnior, A linear programming model for operational optimization of agricultural activity considering a hydroclimatic forecast—case studies for Western Bahia, Brazil, Water 14 (2022) 3625, https://doi.org/10.3390/w14223625.
[10] L. Chen, M. Yang, X. Liu, X. Lu, Attribution and sensitivity analysis of runoff variation in the yellow river basin under climate change, Sustainability 14 (2022), 14981, https://doi.org/10.3390/su142214981.
[11] L. Di Matteo, A. Capoccioni, M. Porreca, C. Pauselli, Groundwater-surface water interaction in the Nera River Basin (Central Italy): new insights after the 2016 seismic sequence, Hydrology 8 (2021) 97, https://doi.org/10.3390/hydrology8030097.
[12] M.O. Schwartz, J. Kgomanyane, Modelling natural attenuation of heavy-metal groundwater contamination in the Selebi-Phikwe mining area, Botswana, Environ. Geol. 54 (2008) 819–830.
[13] H. Yazicigil, C. Er, J.S. Ates, M.Z. Camur, Effects of solution mining on groundwater quality in the Kazan trona field, Ankara-Turkey: model predictions, Environ. Geol. 57 (2009) 157–172.
[14] M. Lghoul, A. Maqsoud, R. Hakkou, A. Kchikach, Hydrogeochemical behavior around the abandoned Kettara mine site, Morocco, J. Geochem. Explor. 144 (2014) 456–467, https://doi.org/10.1016/j.gexplo.2013.12.003.
[15] C.J. Gandy, P.L. Younger, Effect of a clay cap on oxidation of Pyrite within mine spoil, Q. J. Eng. Geol. Hydrogeol. 36 (2003) 207–215.
[16] A. Sako, O. Bamba, A. Gordio, Hydrogeochemical processes controlling groundwater quality around Bomboré gold mineralized zone, Central Burkina Faso, J. Geochem. Explor. 170 (2016) 58–71, https://doi.org/10.1016/j.gexplo.2016.08.009.
[17] B. Valfrey-Visser, M. Rama, Rapport pays- Etats des lieux de l'eau et de l'assainissement au niveau national, Livre Bleu BURKINA FASO, deuxième édition, 2012.
[18] R. Yonaba, Spatio-temporal Land Use and Land Cover Dynamics and Impact on Surface Runoff in a Sahelian Landscape: Case of Tougou Watershed (Northern Burkina Faso), PhD Thesis, International Institute for Water and Environmental Engineering (2iE), 2020, https://tel.archives-ouvertes.fr/tel-03119095.
[19] B. Lèye, C.O. Zouré, R. Yonaba, H. Karambiri, Water resources in the Sahel and adaptation of agriculture to climate change: Burkina Faso, in: S. Diop, P. Scheren, A. Niang (Eds.), Climate Change and Water Resources in Africa, Springer International Publishing, Cham, 2021, pp. 309–331, https://doi.org/10.1007/978-3-030-61225-2_14.
[20] L.A. Mounirou, R. Yonaba, M. Koïta, J.-E. Paturel, G. Mahé, H. Yacouba, H. Karambiri, Hydrologic similarity: dimensionless runoff indices across scales in a semi-arid catchment, J. Arid Environ. 193 (2021), 104590, https://doi.org/10.1016/j.jaridenv.2021.104590.
[21] B. Sawadogo, M.D. Faye, Y. Konaté, A.L. Ekoun, G.T. Ayele, H. Karambiri, Physico-chemical and microbial characterisation of water from the Abengourou dam in Eastern Côte d'Ivoire, Am. J. Environ. Protect. 12 (2023) 109–120.
[22] M.S.A. Babaye, I. Sandao, M.B. Saley, I. Wagani, B. Ousmane, Comportement hydrogéochimique et contamination des eaux des aquifères fissurés du socle précambrien en milieu semi-aride (Sud-Ouest du Niger), Int. J. Brain Cognit. Sci. 10 (2016) 2728–2743.
[23] A.A. Mahamane, B. Guel, Caractérisations physico-chimiques des eaux souterraines de la localité de Yamtenga (Burkina Faso), Int. J. Brain Cognit. Sci. 9 (2015) 517–533.
[24] M.D. Faye, A.C. Biaou, D.D. Soro, B. Leye, M. Koita, H. Yacouba, Understanding groundwater pollution of sissili catchment area in BURKINA-FASO, LARHYSS Journal (2020) 121–144. P-ISSN 1112-3680/E-ISSN 2521-9782. 0.

[25] A.E.L. Eba, K.J. Kouamé, J.P. Jourda, G.E. Aké, M.B. Saley, K.A. Anoh, S.K. Deh, Demarcation of surface water protection perimeters by using GIS: case of gagnoa reservoir in west central of Côte d'Ivoire, Int. J. Sci. Eng. Res. 4 (2013) 1311–1320.
[26] A. Yameogo, Y.S.C. Some, A.B. Sirima, D.E.C. Da, Occupation des terres et érosion des sols dans le bassin versant supérieur de la Sissili, Burkina Faso, Afrique Sci. 17 (2020) 43–56.
[27] N. Savadogo, Géologie et hydrogéologie du socle cristallin de Haute-Volta: Etude régionale du bassin versant de la Sissili, Doctoral dissertation, Université scientifique et médicale de Grenoble, France, 1984.
[28] N. Savadogo, Hydrogéologie du bassin versant de la Haute-Sissili (Haute-Volta, Doctoral dissertation, Université scientifique et médicale de Grenoble, France, 1975.
[29] D. Giovenazzo, S. Séjourné, A. Hein K, M. Jébrak, R. Dahl, C. Ouédraogo, F. Ouédraogo, U. Wenmenga, Notice explicative de la carte de synthèse géologique, structurale et des substances minérales du BURKINA FASO à l'échelle 1/1 000 000, l'équipe d'Effigis Géo-Solutions, 2018.
[30] R. Dahl, A. Hein K, S. Séjourné, C. Ouédraogo, D. Giovenazzo, Carte de synthèse géologique, structurale et des substances minérales du BURKINA FASO à l'échelle 1/1 000 000, Effigis Géo-Solutions, 2018.
[31] M.D. Faye, A.C. Biaou, P.A. Doulkom, M. Koita, H. Yacouba, Contribution of remote sensing and geophysical prospecting (1D) to the knowledge of groundwater resources Burkina Faso, Am. J. Water Resour. 11 (2023) 49–64, https://doi.org/10.12691/ajwr-11-2-2.
[32] M. Koita, H. Jourde, D. Ruelland, K. Koffi, S. Pistre, I. Savane, Cartographie des accidents régionaux et identification de leur rôle dans l'hydrodynamique souterraine en zone de socle. Cas de la région de Dimbokro-Bongouanou (Côte d'Ivoire), Hydrol. Sci. J. 55 (2010) 805–820.
[33] N.L. Mouakoumbat, U.M. Gampio, H. Obami-ondon, G.M. Nkaya, R. Niere, Caracterisation hydrogeologique et approche d'un model conceptuel de l'aquifere de la cuvette congolaise, republique du Congo, Annale Des Sciences et Techniques 21 (2022).
[34] I.C. Alle, Évaluation de l'implantation géophysique des forages d'eau en zone de socle en milieu tropical (Bénin, Afrique de l'Ouest): apport de la tomographie de résistivité électrique pour la caractérisation de la cible hydrogéologique, PhD Thesis, Université d'Abomey-Calavi (Bénin), 2019.
[35] S. Buggiarin, M. Rodighiero, P. Ronco, A. Sottani, L. Vettorello, Hydrogeological modelling and water safety plans: basic knowledge for the protection of the resource, Environ. Sci. Proc. 21 (2022) 32, https://doi.org/10.3390/environsciproc2022021032.
[36] D.D. Soro, Caractérisation et modélisation hydrogéologique d'un aquifère en milieu de socle fracturé: cas du site expérimental de Sanon (région du plateau central au Burkina Faso, Thèse de doctorat, Université Pierre et Marie Curie-Paris VI, France, Institut international d'ingénierie de l'eau et de l'environnement, Burkina Faso, 2017.
[37] J. Bear, A. Verruijt, Modeling Groundwater Flow and Pollution, Reidel, Norwell, MA, 1987.
[38] E. Cesar, Modélisation régionale des écoulements souterrains et du transport de nitrates dans le bassin de la Dyle amont, Thèse de doctorat, Université de Liège, Belgique, 2012.
[39] H. Qian, J. Chen, K.W. Howard, Assessing groundwater pollution and potential remediation processes in a multi-layer aquifer system, Environ. Pollut. 263 (2020), 114669.
[40] R. Rusagara, M. Koïta, V. Plagnes, A. Jost, Groundwater recharge pathways to a weathered-rock aquifer system in a dryland catchment in Burkina Faso, Hydrogeol. J. 30 (2022) 1489–1512.
[41] A. Bon, J. Ndam Ngoupayou, G. Ewodo Mboudou, G. Ekodeck, Caractérisation hydrogéologique des aquifères de socle altéré et fissuré du bassin versant de l'Olézoa à Yaoundé, Cameroun, Revue Des Sciences de l'eau/Journal of Water Science 29 (2016) 149–166.
[42] S. Carrière, Modélisation hydrogéologique à grande échelle: choix conceptuels et calibration: exemple du bassin de la Dyle (Belgique), 2010.
[43] K.A. Kouassi, W.F. Kouassi, O.M.J. Mangoua, P. Ackerer, G.A. Douagui, I. Savané, Estimation par approche inverse d'un champ de transmissivité sur l'ensemble de l'aquifère du Continental Terminal (CT) d'Abidjan, Proc. Int. Assoc. Hydrol. Sci. 384 (2021) 49–56.
[44] É. Philippe, Contribution à la modélisation du transfert des nitrates au travers de la zone non saturée à l'échelle régionale: application au bassin de la Seine, phdthesis, École Nationale Supérieure des Mines de Paris, 2011. https://pastel.archives-ouvertes.fr/pastel-00622536. (Accessed 16 November 2022).
[45] A. Haddane, M. Hacini, A. Bellaoueur, Hydrochimie et facies geochimiques des saumures du chott baghdad (sud algerien), 2015.
[46] N. Al-Amri, J. Budiman, A. Elfeki, Integrated surface water and groundwater modeling in arid environment, Al-Lusub Watershed, Saudi Arabia, Water 14 (2022) 3075, https://doi.org/10.3390/w14193075.
[47] Y. Gao, Z. Xu, S. Li, W. Yu, Modeling monthly nitrate concentration in a Karst spring with and without discrete conduit flow, Water 14 (2022) 1622, https://doi.org/10.3390/w14101622.
[48] O.Z. De Lasme, S.D. Kouadio, A. Coulibaly, Caractérisation des propriétés hydrodynamiques des aquifères du socle dans Quelques Localités du nord de La côte d'Ivoire, Eur. Scientif. J., ESJ. 17 (2021) 137–153.
[49] J. Liu, J. Wu, S. Rong, Y. Xiong, Y. Teng, Groundwater vulnerability and groundwater contamination risk in Karst area of Southwest China, Sustainability 14 (2022), 14483, https://doi.org/10.3390/su142114483.
[50] R. Ghasemizadeh, F. Hellweger, C. Butscher, Modélisation de l'écoulement et du transport des eaux souterraines des aquifères karstiques, avec une référence particulière au système aquifère calcaire de la côte nord de Porto Rico, Hydrogeologie 20 (2012) 1441–1461, 10.1007/s10040-012-0897-4.
[51] Z. Xu, B. Hu, J. Cao, Simulating long term nitrate-N contamination processes in the Woodville Karst Plain using CFPv2 with, UMT3D 54 (2015) 72–88, 10.1016/j.jhydrol.2015.02.024.
[52] A. Dassargues, Formation en modélisation hydrogéologique, 2022.
[53] Y. Zong, Using MT3DMS for Simulation of Field-Scale Heat Transport with Groundwater Advection for Applications to Borehole Geothermal Systems, PhD Thesis, 2020.
[54] S. Yan, A.J. Valocchi, Flux-corrected transport with MT3DMS for positive solution of transport with full-tensor dispersion, Groundwater 58 (2020) 338–348.
[55] M.R. Balf, R. Noori, R. Berndtsson, A. Ghaemi, B. Ghiasi, Evolutionary polynomial regression approach to predict longitudinal dispersion coefficient in rivers, J. Water Supply Res. Technol. - Aqua 67 (2018) 447–457.
[56] W. Zhou, C.W. Lim, Topological edge modeling and localization of protected interface modes in 1D phononic crystals for longitudinal and bending elastic waves, Int. J. Mech. Sci. 159 (2019) 359–372.
[57] K.O. Baek, I.W. Seo, Modifying elder's longitudinal dispersion coefficient for two-dimensional solute mixing analysis in open-channel bends, Water 14 (2022) 2962, https://doi.org/10.3390/w14192962.
[58] H. Jarray, M. Zammouri, M. Ouessar, Assessment of groundwater salinization using PEST and sensitivity analysis: case of Zeuss-Koutine and Mio-Plio-Quaternary aquifers, Arabian J. Geosci. 13 (2020) 1–16.
[59] T. Kurasawa, M. Suzuki, K. Inoue, Experimental assessment of solute dispersion in stratified porous media, Hydrol. Res. Lett. 14 (2020) 123–129.
[60] V.Y.B. Loyara, R. Guillaume Bagré, D. Barro, Estimation of the value at risk using the stochastic approach of taylor formula, Int. J. Math. Math. Sci. 2020 (2020), e6802932, https://doi.org/10.1155/2020/6802932.
[61] D. Fantazzini, Copula's Conditional Dependence Measures for Portfolio Management and Value at Risk, L. Bauwers Y W. Pohlmeier, Summer School in Economics and Econometrics of Market Microstructure, Universidad de Constanza, 2004.
[62] V.Y.B. Loyara, R. Bagre, F. Bere, Estimated of COVID-19 sampling mean in Burkina Faso, J. Math. Res. 12 (2020) p25, https://doi.org/10.5539/jmr.v12n4p25.
[63] R.G. Bagré, V.Y.B. Loyara, D. Barro, Spatial characterization of stochastic dependence using copulas, Far East J. Theor. Stat. 58 (2020) 21–35.
[64] J. Carreau, Y. Bengio, Estimation de densité conditionnelle lorsque l'hypothèse de normalité est insatisfaisante, 2004, pp. 343–6804.
[65] H. Joe, Multivariate Models and Multivariate Dependence Concepts, CRC press, 1997.
[66] M. Hofert, Sampling Nested Archimedean Copulas with Applications to CDO Pricing, PhD Thesis, Universität Ulm, 2010.
[67] U. Cherubini, E. Luciano, W. Vecchiato, Copula Methods in Finance, John Wiley & Sons, 2004.
[68] J. Lee, A. Prékopa, Properties and calculation of multivariate risk measures: MVaR and MCVaR, Ann. Oper. Res. 211 (2013) 225–254.

[69] F.C. Brassington, P.L. Younger, A proposed framework for hydrogeological conceptual modelling, Water Environ. J. 24 (2010) 261–273.
[70] L. Chen, M. Yang, X. Liu, X. Lu, Attribution and sensitivity analysis of runoff variation in the yellow river basin under climate change, Sustainability 14 (2022), 14981, https://doi.org/10.3390/su142214981.
[71] R. Yonaba, L.A. Mounirou, F. Tazen, M. Koïta, A.C. Biaou, C.O. Zouré, P. Queloz, H. Karambiri, H. Yacouba, Future climate or land use? Attribution of changes in surface runoff in a typical Sahelian landscape, Compt. Rendus Geosci. 355 (2023) 1–28.